Inorganic Chemistry

Article

pubs.acs.org/IC

Interaction of Chromium(III) with a *N,N′*-Disubstituted Hydroxylamine-(diamido) Ligand: A Combined Experimental and Theoretical Study

Petros A. Tziouris,[†] Constantinos G. Tsiafoulis,[#] Manolis Vlasiou,[‡] Haralampos N. Miras,*[,§] Michael P. Sigalas,*[,⊥] Anastasios D. Keramidas,*[,‡] and Themistoklis A. Kabanos*[,†]

[†]Section of Inorganic and Analytical Chemistry, Department of Chemistry and [#]NMR Center, University of Ioannina, Ioannina 45110, Greece

[‡]Department of Chemistry, University of Cyprus, Nicosia 1678, Cyprus

[§]WestCHEM, School of Chemistry, The University of Glasgow, Glasgow G12 8QQ, U.K.

[⊥]Laboratory of Applied Quantum Chemistry, Department of Chemistry, Aristotle University of Thessaloniki, Thessaloniki 54124, Greece

Supporting Information

ABSTRACT: Reaction of hydroxylamine hydrochloride with prop-2-enamide in dichloromethane in the presence of triethylamine resulted in the isolation of the *N,N′*-disubstituted hydroxylamine-(diamido) ligand, 3,3′-(hydroxyazanediyl)dipropanamide (Hhydia). The ligand Hhydia was characterized by multinuclear NMR, high-resolution electrospray ionization mass spectrometry (ESI-MS), and X-ray structure analysis. Interaction of Hhydia with *trans*-$[Cr^{III}Cl_2(H_2O)_4]Cl{\cdot}2H_2O$ in ethanol yields the ionization isomers $[Cr^{III}(Hhydia)_2]Cl_3{\cdot}2H_2O$ (**1**·$2H_2O$) and *cis/trans*-$[Cr^{III}Cl_2(Hhydia)_2]Cl{\cdot}2H_2O$ (**2**·$2H_2O$). The X-ray structure analysis of **1** revealed that the chromium atom in $[Cr^{III}(Hhydia)_2]^{3+}$ is bonded to two neutral tridentate *O,N,O*-Hhydia ligands. The twist angle, *θ*, in $[Cr^{III}(Hhydia)_2]^{3+}$ is $54.5(6)^0$, that is, very close to an ideal octahedron. The intramolecular hydrogen bonds developed between the N−OH group of the first ligand and the amidic oxygen atom of the second ligand and vice versa contribute to the overall stability of the cation $[Cr^{III}(Hhydia)_2]^{3+}$. The reaction rate constant of the formation of Cr(III) complexes **1**·$2H_2O$ and **2**·$2H_2O$ was found to be $8.7(\pm0.8) \times 10^{-5}$ M^{-1} s^{-1} at 25 °C in methyl alcohol and follows a first-order law kinetics based on the biologically relevant ligand Hhydia. The reaction rate constant is considerably faster in comparison with the corresponding water exchange rate constant for the hydrated chromium(III). The modification of the kinetics is of fundamental importance for the chromium(III) chemistry in biological systems. Ultraviolet-visible and electron paramagnetic resonance studies, both in solution and in the solid state, ESI-MS, and conductivity measurements support the fact that, irrespective of the solvent used in the interaction of Hhydia with *trans*-$[Cr^{III}Cl_2(H_2O)_4]Cl{\cdot}2H_2O$, the ionization isomers$[Cr^{III}(Hhydia)_2]Cl_3{\cdot}2H_2O$ (**1**·$2H_2O$) and *cis/trans*-$[Cr^{III}Cl_2(Hhydia)_2]Cl{\cdot}2H_2O$ (**2**·$2H_2O$) are produced.The reaction medium affects only the relevant percentage of the isomers in the solid state. The thermodynamic stability of the ionization isomers **1**·$2H_2O$ and *cis/trans*-**2**·$2H_2O$, their molecular structures as well as the vibrational spectra and the energetics of the Cr^{III}− Hhydia/$hydia^-$ were studied by means of density functional theory calculations and found to be in excellent agreement with our experimental observations.

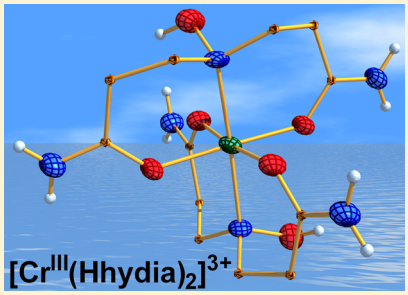

INTRODUCTION

Chromium is the sixth most abundant element in the earth's crust and has numerous applications in the chemical industry, pigments, wood preservation, leather tanning, electroplating, ceramics, and manufacturing of various alloys.[1] Chromium(VI) species, such as $Cr^{VI}O_4^{2-}$ and $Cr^{VI}_2O_7^{2-}$, are carcinogenic and mutagenic agents.[2] Workers exposed to chromium dust show a high percentage of lung and other bronchial cancers.[2] Since reactions between Cr(VI) or Cr(III) and DNA have shown insignificant damage to DNA,[3] it is believed that metastable hypervalent Cr(IV/V) species generated in the cellular milieu cause DNA damage and mutations.[4,5] In fact, reductants such as glutathione,[3,6] ascorbic acid,[7] and cytochrome P-450[8] indeed reduce Cr(VI) to Cr(III) through detectable Cr(V) and Cr(IV) intermediates. Moreover, highly reactive Cr(IV/V) species and organic radicals are also formed in the oxidation reactions of Cr(III) to Cr(VI) with biological oxidants such as ClO^-, H_2O_2, lipid peroxidases, etc.[9]

In marked contrast to all the other transition metals that are regarded as essential for some form of life (V, Mn, Fe, Co, Ni, Cu, Zn, Mo, and W), no Cr-containing biomolecules have been definitively characterized as yet[10] in terms of their structures or the mode of action. Concerning the application of chromium-

Received: May 13, 2014
Published: October 20, 2014

   dx.doi.org/10.1021/ic501778d | Inorg. Chem. 2014, 53, 11404−11414

(III) compounds as nutritional supplements or antidiabetic drugs, particularly $[Cr^{III}(pic)_3]$ (pic = 2-pyridinecarboxylate), which was widely used[11] as such, there is a controversy since there is growing concern over the low efficacy and potential toxicity of such supplements.[12] At this point, it is worth pointing out that the synthesis and the structural and physicochemical characterization of chromium(III) compounds in both solution and solid state with amino acids, peptides, proteins, and in general with biological ligands is limited,[13] and thus, the exploration of such chemistry will add valuable information in the interaction of the kinetically inert chromium(III) with biological systems.

Over the past few years, our group has studied vanadium and molybdenum compounds bearing chelating *N*,*N*′-disubstituted-(hydroxylamino) ligands,[14] inspired by the naturally occurring vanadium compound in mushrooms of the genus Amanita,[15] where the chelating *N*,*N*′-disubstituted-(hydroxylamino) ligand *N*-hydroxy-*α*,*α*′-iminodipropionate, hidpa^{3-}, (Scheme 1) binds

Scheme 1

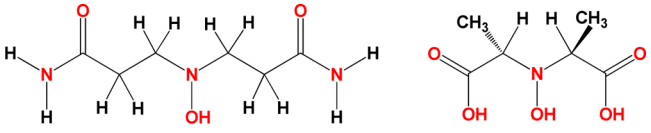

very tightly to vanadium.[15] During the course of this research, it became clear that this kind of ligand gives very thermodynamically stable complexes and a very rich chemistry.[14] Hydroxylamines have also attracted our attention because they are selective antibacterial agents,[16] strong antioxidants,[17] drug metabolites,[18] effective to metal detoxification,[19] and have antidiabetic activity,[20] and their ligation to antidiabetic metal ions, such as vanadium(V), enhances their antidiabetic activity.[21]

Therefore, continuing our program of designing new *N*,*N*′-disubstituted(hydroxylamino) potentially chelating ligands, the *N*,*N*′-disubstituted(hydroxylamino) chelating ligand 3,3′-(hydroxyazanediyl)dipropanamide (Hhydia) (Scheme 1) was synthesized, and its interaction with chromium(III) was explored.

The hydroxylamine ligand Hhydia incorporates the amide functionality, and to our knowledge, this is the first example of a ligand with the coexistence of these two biological functionalities (Scheme 1). Moreover, the organic molecule Hhydia is an antioxidant and prevents the oxidation of various organic materials even in the presence of oxygen or ozone.[22] It is well-known that antioxidants inhibit oxidation of molecules that are vital for cellular processes and protect the cells from oxidative stress-mediated damage.[23] Oxidative stress is a critical component of diseases such as neuronal disease, sickle cell disease, heart malfunction, diabetes, etc.[24]

Herein, we report on the synthesis and the structural and physicochemical characterization (UV−vis, electron paramagnetic resonance (EPR), IR, mass spectrometry (MS), and conductivity) of the ligand Hhydia and its chromium(III) compound $[Cr^{III}(Hhydia)_2]Cl_3{\cdot}H_2O$. The molecular structures, vibrational spectra, and the energetics of the Cr(III)−Hhydia/hydia$^-$ interaction were also studied by means of density functional theory (DFT) calculations.

EXPERIMENTAL SECTION

Materials. *trans*-$[Cr^{III}Cl_2(H_2O)_4]Cl{\cdot}2H_2O$, hydroxylamine hydrochloride, prop-2-enamide, and triethylamine were purchased from Merck. All the solvents were analytical reagent grade and used without further purification. Merck silica gel 60F254 TLC plates were used for thin layer chromatography. C, H, N, Cl, and Cr analyses were conducted by the microanalytical service of the School of Chemistry, the University of Glasgow. For further experimental details see pages S22−S24 in the Supporting Information.

3,3′-(Hydroxyazanediyl)dipropanamide (Hhydia). To a degassed dichloromethane solution (∼40 mL) was added hydroxylamine hydrochloride (4.000 g, 57.56 mmol), prop-2-enamide (8.179 g, 115.1 mmol), and 8.03 mL of triethylamine (5.824 g, 57.56 mmol) under magnetic stirring. The solution cleared 10 min later, and after a while a white precipitate was formed. The reaction mixture was stirred at room temperature (∼25 °C) for 2 h, and then, it was filtered to get a white solid. The crude product was recrystallized from ethyl alcohol (70 mL) and dried in vacuum to afford Hhydia as a crystalline white solid (yield: 7.500 g, 82%). Mp 133−135 °C. High-resolution electrospray ionization(+) (HR-ESI(+))-MS: calcd for $C_6H_{14}N_3O_3$ ($[M + H]^+$) 176.1030, found 176.1021. Anal. Calcd (%) for $C_6H_{13}N_3O_3$: C, 41.12; H, 7.48; N, 23.99. Found (%): C, 41.10; H, 7.54; N, 23.71. ^{1}H NMR (500 MHz, deuterated dimethyl sulfoxide (DMSO-d_6)): δ 2.31 (*t*, 4H, *J* = 6.9 Hz), 2.77 (*t*, 4H, *J* = 6.9 Hz), 7.80 (*s*, 1H, NO**H**), 7.31 (*s*, 2H, CON**H**$_2$), 6.78 (*s*, 2H, CON**H**$_2$). ^{13}C NMR (500 MHz, DMSO-d_6): 33.4, 56.2, 173.3. IR (KBr, 4000−370 cm^{-1}): 3406 (m), 2844 (m), 1660 (s,br), 1620 (m), 1471 (m), 1455 (w), 1435 (w), 1402 (s), 1323 (w), 1290 (m), 1261 (w), 1213 (s), 1137 (s), 1093 (m), 1061 (m), 1035 (s), 996 (w), 895 (w), 842 (m), 817 (m), 768 (m,br), 680 (w), 638 (w), 586 (s), 509 (s), 485 (s) cm^{-1}. R_f = 0.32 ($CH_3COOC_2H_5$/CH_3OH 2:1).

Bis-[3,3′-(hydroxyazanediyl)dipropanamide-*O*,*N*,*O*]-chromium(III) Chloride, $[Cr^{III}(Hhydia)_2]Cl_3{\cdot}2H_2O$, 1·2H$_2$O; *cis*/*trans*-Dichloro-bis-[3,3′-(hydroxyazanediyl)dipropanamide-*O*,*N*]chromium(III) Chloride, *cis*/*trans*-$[Cr^{III}Cl_2(Hhydia)_2]Cl{\cdot}2H_2O$, *cis*/*trans*-2·2H$_2$O. To a stirred solution of *trans*-$[Cr^{III}Cl_2(H_2O)_4]Cl{\cdot}2H_2O$ (0.304 g, 1.14 mmol) in ∼10 mL of ethanol 95% was added solid Hhydia (0.402 g, 2.28 mmol) in one portion. Upon addition of the ligand the green color of the solution changed to deep green and, after approximately half an hour, to a pink color with concomitant formation of a pink precipitate. After the solution was stirred for an additional 2 h, the precipitate was removed by filtration and dried in vacuo. Yield: 0.385 g {60% based on *trans*-$[Cr^{III}Cl_2(H_2O)_4]Cl{\cdot}2H_2O$}. Anal. Calcd (%) for **1**·2H$_2$O [$C_{12}H_{30}Cl_3N_6O_8Cr$(544.63)]: C, 26.44; H, 5.55; Cl, 19.53; N, 15.43; Cr, 9.55. Found (%): C, 26.56; H, 5.35; Cl, 20.03 ; N, 14.81; Cr, 9.50. IR (KBr, 4000−650 cm^{-1}): 3255 (w,b), 3084 (w), 1667 (s), 1554(s), 1480 (m), 1438 (w), 1418 (w), 1396 (m), 1350 (w), 1335 (w), 1296 (m), 1259 (m), 1215 (w), 1197 (w), 1147 (s), 1103 (m), 1049 (w), 997 (s), 970 (s), 900 (s), 834 (s), 786 (m), 722 (m), 674 (w), 595 (s), 530 (w), 509 (w), 475 (w), 417 (m). Crystals of $[Cr^{III}(Hhydia)_2]Cl_3{\cdot}H_2O$ (**1**·H$_2$O) suitable for X-ray structure analysis were obtained as follows: A solution of Hhydia (0.114 g, 0.647 mmol) in 6.0 mL of CH_3OH was mixed with a solution of *trans*-$[Cr^{III}Cl_2(H_2O)_4]Cl{\cdot}2H_2O$ (0.172 g, 0.647 mmol) in 6.0 mL CH_3OH, and it was stirred at room temperature for 5 min. This solution was layered with $(C_2H_5)_2O$, and brick-red crystals were formed after 2 d. Yield: 0.080 g, (24% based on $CrCl_3{\cdot}6H_2O$). Anal. Calcd (%) for **1**·H$_2$O [$C_{13}H_{30}Cl_3N_6O_7Cr$(540.64)]: C, 28.86; H, 5.59; Cl, 19.67; N, 15.54; Cr, 9.61. Found (%): C, 28.56; H, 5.53; Cl, 20.03; N, 15.57; Cr, 9.58.

3,3′-(Hydroxyazanediyl)dipropanamide hydrochloride (H_2hydia$^+$ Cl$^-$·0.5 H$_2$O). To a stirred solution of *trans*-$[Cr^{III}Cl_2(H_2O)_4]Cl{\cdot}2H_2O$ (0.304 g, 1.14 mmol) in ∼10 mL of methyl alcohol was added solid Hhydia (0.402 g, 2.28 mmol) in one portion. Upon addition of the ligand the green color of the solution changed to deep green, to a deep brick-red after approximately half an hour, and finally to a light violet. After the solution was stirred for an additional 2 h, a white precipitate was formed, which was removed by filtration and dried in vacuo. Yield: 0.385 g (80% based on Hhydia). Anal. Calcd (%) for $C_6H_{15}ClN_3O_{3.5}$(220.60): C, 32.64; H, 6.85; Cl, 16.07; N, 19.05.

dx.doi.org/10.1021/ic501778d | *Inorg. Chem.* 2014, 53, 11404−11414

Found (%): C, 32.67; H, 6.75; Cl, 16.03 ; N, 18.81.Mp 133−135 °C. HR-ESI(+)-MS: calcd for $C_6H_{14}N_3O_3$ ($[M - Cl - 0.5\ H_2O]^+$) 176.1030, found 176.1025. ^{1}H NMR (500 MHz, DMSO-d_6): δ 2.69 (*t*, 4H, J = 7.2 Hz), 3.44 (*t*, 4H, J = 7.2 Hz), 7.14 (*s*, 2H, CONHα), 7.69 (*s*, 2H, CONHα'), 11.69 (*s*, 1H,NOH). ^{13}C NMR (500 MHz, DMSO-d_6): 28.60, 53.93, 170.73.IR (KBr, 4000−370 cm^{-1}): 3418 (m), 3301 (m), 3091 (m), 2988 (m), 2897 (m), 2710 (m), 2611 (w), 1678 (s), 1594 (s), 1455(w), 1413 (s), 1368 (m), 1332 (m), 1298 (w), 1249 (w), 1219 (m), 1082 (w), 1068 (w), 1032 (w), 970 (w), 889 (m), 849 (m), 802 (m), 590 (s), 540 (m), 511 (m), 473 (m).

RESULTS AND DISCUSSION

Syntheses. The *N,N′*-disubstituted hydroxylamine-(diamido) ligand, 3,3′-(hydroxyazanediyl)dipropanamideligand, Hhydia, was synthesized with substantial modifications of the literature[22] reported synthesis to increase the yield (~90% vs 50%) and to reduce the time of the reaction (2 h vs 12 h). The synthesis of the ligand Hhydia and its chromium(III) ionization isomers $[Cr^{III}(Hhydia\text{-}O,N,O)_2]Cl_3$ (**1**) and *cis/trans*-$[Cr^{III}Cl_2(Hhydia\text{-}O,N)_2]Cl$ ($\mathbf{2}_{cis/trans}$) are shown in Scheme 2.

Scheme 2. Synthesis of the Ligand Hhydia and Its Chromium(III) Compounds 1 and $\mathbf{2}_{cis/trans}$

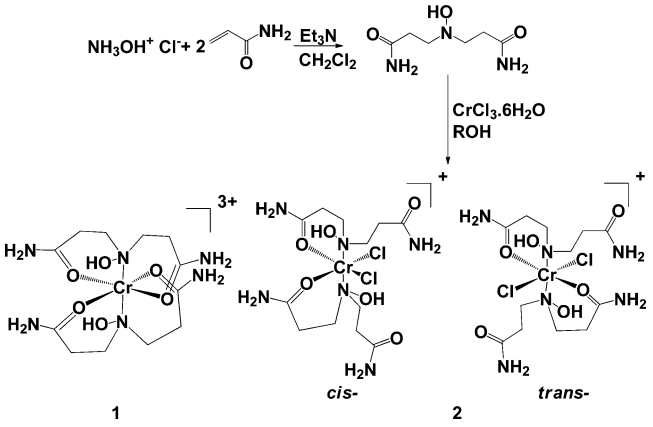

Reaction of *trans*-$[Cr^{III}Cl_2(H_2O)_4]Cl{\cdot}2H_2O$ with the ligand Hhydia in various solvents (ethyl alcohol, isopropanol, and methyl alcohol/diethyl ether) resulted always in the isolation of mixtures of **1** and **2**. Efforts to isolate pure $[Cr^{III}(Hhydia\text{-}O,N,O)_2]^{3+}$ $(SbF_6)_3$ and not the mixture of **1** and $\mathbf{2}_{cis/trans}$, by reacting first *trans*-$[Cr^{III}Cl_2(H_2O)_4]Cl{\cdot}2H_2O$ with 3 equiv of $AgSbF_6$ to remove the chlorine atoms, followed by 2 equiv of the ligand Hhydia, were unsuccessful. Crystals of $[Cr^{III}(Hhydia)_2]Cl_3{\cdot}H_2O$ ($\mathbf{1}{\cdot}H_2O$) were obtained by layering diethyl ether into a freshly prepared methyl alcohol solution containing *trans*-$[Cr^{III}Cl_2(H_2O)_4]Cl{\cdot}2H_2O$ and Hhydia in a molar ratio of 1:1 (changing the molar ratio to 1:2, the crystals were contaminated with the ligand Hhydia). The crystalline material obtained in this way contains single crystals of $\mathbf{1}{\cdot}H_2O$ and the ionization isomers *cis/trans*-$[Cr^{III}Cl_2(Hhydia\text{-}O,N)_2]Cl$ ($\mathbf{2}_{cis/trans}$). Treatment of *trans*-$[Cr^{III}Cl_2(H_2O)_4]Cl{\cdot}2H_2O$ with 2 equiv of Hhydia in either ethyl alcohol or isopropyl alcohol yielded also mixtures of the ionization isomers **1** and $\mathbf{2}_{cis/trans}$, while in the case of methyl alcohol the protonated form of the ligand, H_2hydia^+ Cl^-, was isolated, as it was evidenced by HR ESI(+) MS, elemental analysis, and multinuclear NMR. When isopropyl alcohol was used as a solvent the yield of the reaction was almost 100%, since compounds **1** and $\mathbf{2}_{cis/trans}$ are insoluble in this solvent. Despite of all our trials to separate the crystals of **1** from those of **2**, this was not possible because of the nature of the crystalline material, which was a polycrystalline aggregate. In addition, the isomers were not separated on TLC using for mobile phase methyl alcohol or mixtures of methyl alcohol/isopropanol.

Crystal Structures. A perspective view of the structure of the ligand Hhydia with the numbering scheme used is shown in Figure 1. Interatomic distances and bond angles are listed in Supporting Information, Table S2. The conformation of the ligand is the most thermodynamically stable as predicted by the theory (vide infra), though the conformation of the chromium-bound ligand is only slightly higher in energy (6.7 kJ mol^{-1}). The N−OH bond length of 1.451(2) Å is almost identical to the bond length of 1.453 Å in the gas-phase hydroxylamine.[25] The two amide groups are planar within the limits of precision. The mean d(C═O) and d(C−N) values of 1.241(2) and 1.329(3) Å, respectively, are in the expected range.[26] Moreover, there is an extended hydrogen-bonding network in the solid state (Supporting Information, Figure S1). Each of the organic molecules is connected via an extended network of hydrogen bonds, O(1)−H···N(1) {$d_{O(1)-N(1)}$ = 2.846(2) Å}, N(2)−H···O(2), and N(3)−H···O(3) {$d_{O(2)-N(2)}$ = 2.940(3), $d_{O(3)-N(3)}$ = 2.894(3) Å}, N(2)−-H···O(3), and N(3)−H···O(2) {$d_{O(3)-N(2)}$ = 2.976(3), $d_{O(2)-N(3)}$ = 2.979(3) Å} to seven neighboring molecules constructing a three-dimensional (3D) structure.

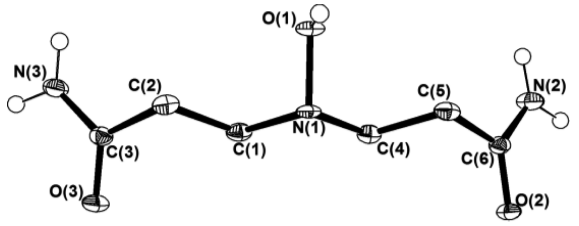

Figure 1. ORTEP diagram of the ligand Hhydia with atomic numbering scheme and thermal ellipsoids at 50% probability level. The methylene hydrogen atoms were omitted for clarity.

The molecular structure of the cation $[Cr^{III}(Hhydia)_2]^{3+}$ is shown in Figure 2. A selection of interatomic distances and bond angles is listed in Supporting Information, Table S3. The chromium atom in $[Cr^{III}(Hhydia)_2]^{3+}$ is bonded to two neutral tridentate Hhydia ligands, and each of the two Hhydia ligands acts as a tridentate *O,N,O* donor (Figure 2). The chromium-

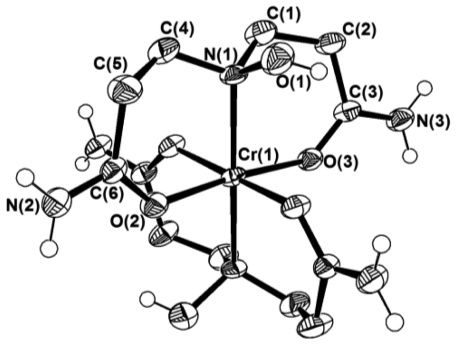

Figure 2. ORTEP diagram of $[Cr^{III}(Hhydia)_2]^{3+}$ with atomic numbering scheme and thermal ellipsoids at 50% probability level. The methylene hydrogen atoms, Cl^- counterions, and crystal lattice H_2O molecules were omitted for clarity. Selected bond distances (Å): N(1)−Cr(1), 2.117(3); O(2)−Cr(1), 1.959(3); and O(3)−Cr(1), 1.950(3) Å.

dx.doi.org/10.1021/ic501778d | Inorg. Chem. 2014, 53, 11404−11414

(III) atom is an inversion center in the cation $[Cr^{III}(Hhydia)_2]^{3+}$. The donor atoms surrounding the chromium ion are disposed in an octahedral geometry where four carbonyl oxygen atoms of two different ligand molecules occupy the equatorial plane, and the two *trans*-hydroxylamine nitrogen atoms occupy the axial positions. The four amide functionalities are planar within the limits of precision. Each of the two Hhydia ligands forms two six-membered fused chelate rings and is meridionally ligated to the chromium center.

Upon coordination of the ligand Hhydia to chromium(III), the N−OH and C−O_{amide} bonds are weakened and lengthened-(N−OH, from 1.451 to 1.472 and C═O_{amide}, from 1.239 and 1.243 to 1.267 and 1.281 Å, respectively), while the C−N_{amide} bond is strengthened and shortened (C−N_{amide}, from 1.326 and 1.332 to 1.296 and 1.300 Å, respectively). Concerning the amide group this means a larger contribution of the ionic resonance structure (Scheme 3).

Scheme 3

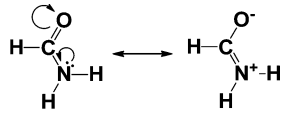

The two planes defined by the three donor atoms (*O,N,O*) of each ligand are found to be perpendicular to one another with a dihedral angle of 88.0(1)^0. The average Cr−O_{amide} bond length [1.955(3) Å] is almost identical to the reported mean Cr−O_{amide} value[27] [1.951(3) Å] for the two other chromium(III)-organic amide structures reported.[27] The (Cr−$N_{hydroxylamine}$) bond length [2.117(3) Å] is reasonable for a Cr−N (sp^3) dative bond. The N(1)−Cr(1)−N(1)# axis is close to linearity [174.3(2)^0], and so are the O(2)−Cr(1)−O(3) [173.9(2)^0] and #O(2)−Cr(1)−O(3)# [173.9 (1)^0] axes. The twist angle (θ)[28] in $[Cr^{III}(Hhydia)_2]^{3+}$ is 54.5(6)^0, that is, very close to ideal octahedron. There are two intramolecular hydrogen bonds in $[Cr^{III}(Hhydia)_2]^{3+}$ between the hydrogen atom attached to $O_{hydroxylamine}$ of one ligand and the amide oxygen atom of the other ligand and vice versa (Figure 11 and Supporting Information, Figure S2). These two hydrogen bonds contribute to the overall stability of the $[Cr^{III}(Hhydia)_2]^{3+}$ cationic complex.

Moreover, X-ray diffraction analysis revealed the existence of an extended network of hydrogen bonds leading to

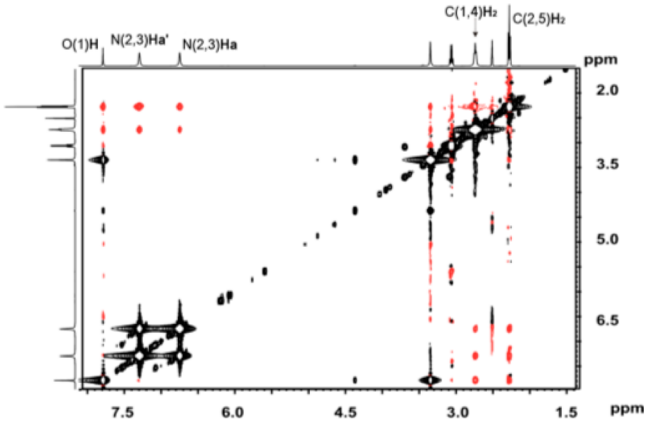

Figure 3. 2D {^{1}H, ^{1}H} NOESY spectrum of a DMSO-d_6 solution of Hhydia, (mixing time used 0.3 s) at 500 MHz.

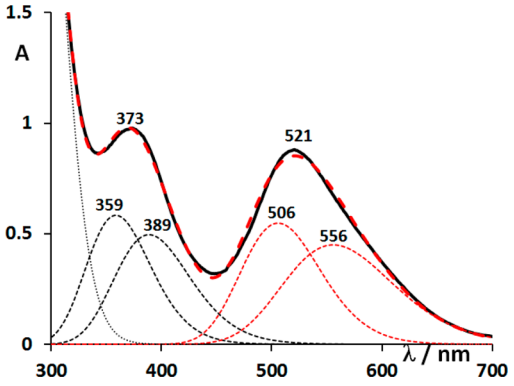

Figure 4. Deconvolution of the experimental (black line) and simulated (red thick dashed line) UV−visible spectrum of **1**·H_2O[29a] in CH_3OH (11.30 mM). The peak at 521 nm was fitted using two peaks at 506 and 556 nm (red dotted lines), while the peak at 373 nm was fitted using two peaks at 359 and 389 nm (black dotted lines).

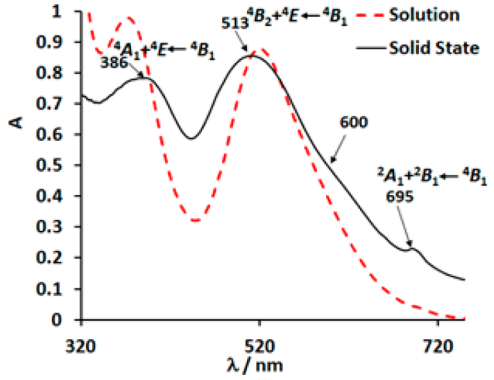

Figure 5. UV−visible spectrum of **1**·H_2O[29a] in CH_3OH (11.30 mM, red dashed line) and its solid-state diffuse reflectance spectrum (black solid line).

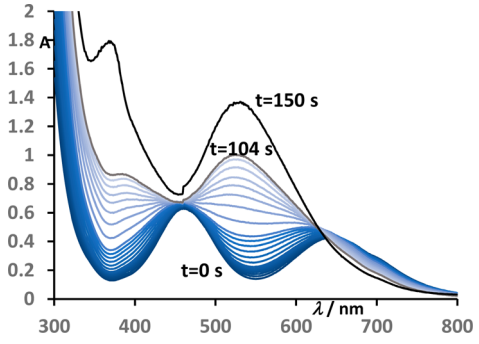

Figure 6. UV−visible spectra of a solution of *trans*-$[Cr^{III}Cl_2(H_2O)_4]$-Cl·2H_2O (22.2 mM) and Hhydia (72.0 mM) in CH_3OH at 25 °C measured every 15 s.

intermolecular interactions (see Supporting Information, Figure S3). The hydrogen bonds formed between the N(2) amide nitrogen with the free water molecule O(4), N(2)−H2···O(4) {*d*[N(2)−O(4)] = 2.894(4) Å}, and the Cl(1) anion, N(2)−H2···Cl(1) {*d*[N(2)−Cl(1)] = 3.096(3) Å}, trigger the formation of one-dimensional chains of dimers along the *c* axis. The strips are parallel to each other and are connected further though weaker hydrogen bonds between the Cl(2) and the amido hydrogens of N(3) into an overall 3D architecture.

At this point, it is worth noting that the ligand Hhydia behaves as a tridentate *O,N,O* donor forming two fused six-

dx.doi.org/10.1021/ic501778d | *Inorg. Chem.* 2014, 53, 11404−11414

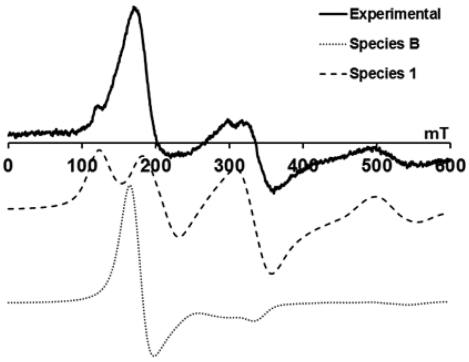

Figure 7. X-band EPR spectrum of $\mathbf{1}\cdot H_2O$[29a] in CH_3OH (1.0 mM, black line) at 120 K, microwave resonance = 9.43 GHz, and the simulated spectra of two species taken into account for the spectrum simulation: Species B (black dot line), with g = 1.97, D = 11718 MHz (0.391 cm^{-1}), E = 188 MHz (0.006 cm^{-1}) (weight 45%), E/D = 0.05 and species $\mathbf{1}$[29b] (black dashed line), with g = 1.97, D = 8312 MHz (0.277 cm^{-1}), E = 2658 MHz (0.0887 cm^{-1}), E/D = 0.32 (weight 55%).

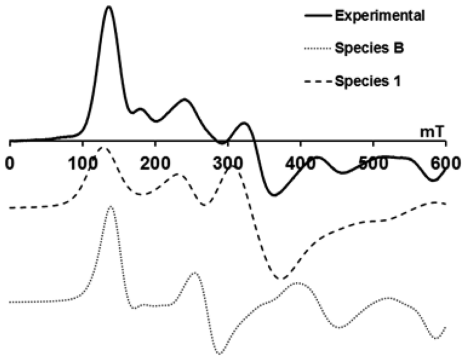

Figure 8. X-band powder EPR spectrum of $\mathbf{1}\cdot H_2O$[29a] (black line) at 120 K, microwave resonance = 9.43 GHz, and the simulated spectra of two species taken into account for the spectrum simulation: Species B, (black dot line), with dashed line, $g_{//}$ = 1.957, $g_{\perp}$ = 1.987 D = 7952 MHz (0.265 cm^{-1}), E = 1736 MHz (0.0579 cm^{-1}), E/D = 0.22 (weight 30%) and species $\mathbf{1}$,[29b] dashed line, $g_{//}$ = 1.956, $g_{\perp}$ = 1.987 D = 9414 MHz (0.314 cm^{-1}), E = 3006 MHz (0.100 cm^{-1}), E/D = 0.32 (weight 70%).

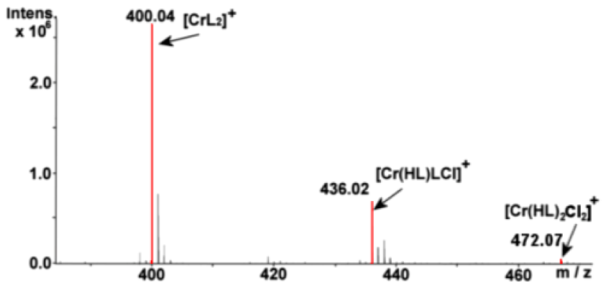

Figure 9. Positive ion mass spectra of $\mathbf{1}\cdot H_2O$[29a] in CH_3OH, showing the isotopic distribution envelopes of $\{[Cr^{III}L_2]\}^+$, $\{[Cr^{III}(HL)LCl\}^+$, and $[Cr^{III}(HL)_2Cl_2]^+$ (where L = hydia$^-$) centered at m/z = 400.04, 436.02, and 472.07, respectively.

membered chelate rings in the chromium(III) complex $[Cr^{III}(Hhydia\text{-}O,N,O)_2]^{3+}$, and the nondeprotonated hydroxylamine group acts as a *N*-bound site (Scheme 6). This observation is in marked contrast to the biological ligand hidpa^{3-} (Scheme 1), which acts as a tetradentate *O,N,O,O* donor forming two fused five-membered chelate rings in its vanadium(IV/V)[15] compounds, with the depronated hydroxylamine group binding in a side-on fashion (Scheme 6).[15]

NMR Spectroscopy. The ^{13}C NMR spectrum of the ligand Hhydia in DMSO-d_6 (Supporting Information, Figure S4 and Table S4) gave three peaks at 33.4, 56.2, and 173.3 ppm, which were assigned to the four methylene, C(2,5) and C(1,4), and the two carbonyl carbon nuclei, C(3,6) (Scheme 4), respectively, on the basis of the two-dimensional (2D) $\{^1H,^{13}C\}$ heteronuclear single quantum correlation and heteronuclear multiple-bond correlation spectra. The ^1H NMR spectrum of Hhydia in DMSO-d_6 (Supporting Information, Figure S5) showed two triplets (4H each) at 2.31 for [C(2,5)$\mathbf{H_2}$] and at 2.77 for [C(1,4)$\mathbf{H_2}$], two singlets for the amide protons at 6.78 [N(2,3)**Ha**Ha′] and at 7.31 ppm [N(2,3)Ha**Ha**′], and a singlet for the hydroxylamine proton [−O(1)**H**] at 7.80 ppm. In marked contrast to the asymmetry of the ligand Hhydia observed in the solid state (Figure 1), the presence of only three peaks in the ^{13}C NMR and the ^1H NMR spectra of Hhydia in DMSO-d_6 indicate that the two propylamide arms of the organic molecule are equivalent (C_s point group) in solution.

Furthermore, the 2D $\{^1H,^1H\}$ nuclear Overhauser effect spectroscopy-exchange spectroscopy (NOESY-EXSY) spectra of the ligand Hhydia (Figure 3) were recorded at different mixing times (0.1, 0.3, and 0.8 s). The J coupling constant [J C(2,5)$\mathbf{H_2}$ − C(1,4)$\mathbf{H_2}$ = 7 Hz] and the distances that were calculated from the integration of the NOESY peaks between the vicinal protons (Supporting Information, Table S5) revealed a gauche conformation of Hhydia in solution which is in agreement with its structure in the solid state (Figure1). The off-diagonal EXSY peaks of the spectra of Hhydia at room temperature reveal one intermolecular exchange between the hydroxylamine proton and the water protons and one intramolecular Ha−Ha′ exchange assigned to the C−N rotation process of the amide bond. Variable-temperature experiments in the temperature range of 296−330 K (experiments at higher temperatures were not performed due to the decomposition of the ligand) resulted in the chemical shift of the amide and hydroxylamine proton peaks. The temperature coefficient $\Delta\delta/\Delta T$ was calculated to be −3.49, −4.91, and −3.42 ppb per K for the *a*, *a*′ amido and the hydroxylamine protons, respectively. The barrier for the rotation of the amide group at the C−N bond is usually high (ca. 92 kJ/mol), and in the temperature range of 296−330 K the rate of this process is slow. Thus, the chemical shift of the amide protons with the temperature must be attributed mainly to their hydrogen bonds with the solvent molecules. The more negative temperature coefficient of the H*a*′ amide protons indicates the formation of stronger hydrogen bonds between them and the solvent molecules than between the H*a* amide protons and the solvent molecules. This is in agreement with the solid-state structure of the ligand where the N(2)H*a*′···O(2) and N(3)H*a*′···O(3) distances, [2.939(2) and 2.894(2) Å], are significantly shorter in comparison with the relevant hydrogen bonds of the H*a* protons, [N(2)H*a*···O(2) and N(3)H*a*···O(3) = 2.976(2) and 2.979(2) Å, respectively], leading in the former case to presumably stronger hydrogen bonds.

The ^1H and ^{13}C NMR spectra of $H_2hydia^+Cl^-$ were recorded in DMSO-d_6. The protonation of the neutral Hhydia results in a significant shift of all the ^1H peaks to lower field; more specifically, the triplet peak of the $-C(1)H_2$ protons (Scheme 4) exhibits a larger shift (0.67 ppm) than the $-C(2)H_2$ (0.38 ppm) and $-NH_2$ (0.36 and 0.38 ppm for H_a and H_a',

dx.doi.org/10.1021/ic501778d | *Inorg. Chem.* 2014, 53, 11404−11414

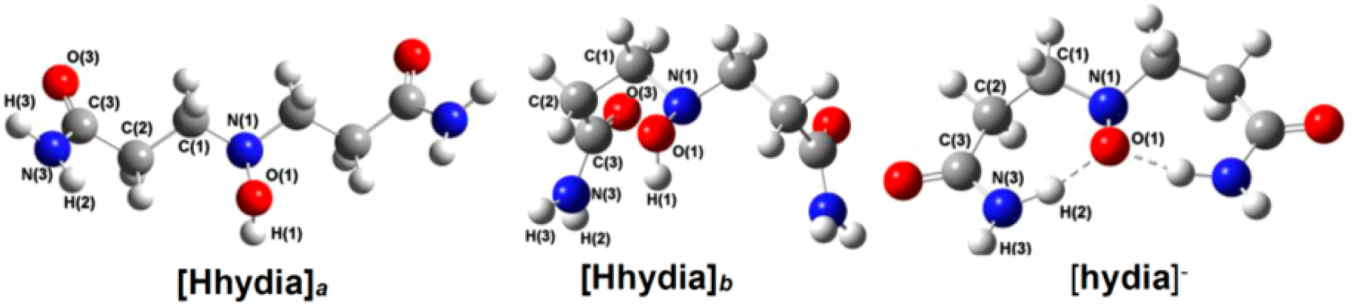

Figure 10. Optimized geometries of the ligand Hhydia {conformations $[Hhydia]_a$ and $[Hhydia]_b$} and its deprotonated form $[hydia]^-$ at the B3LYP level.

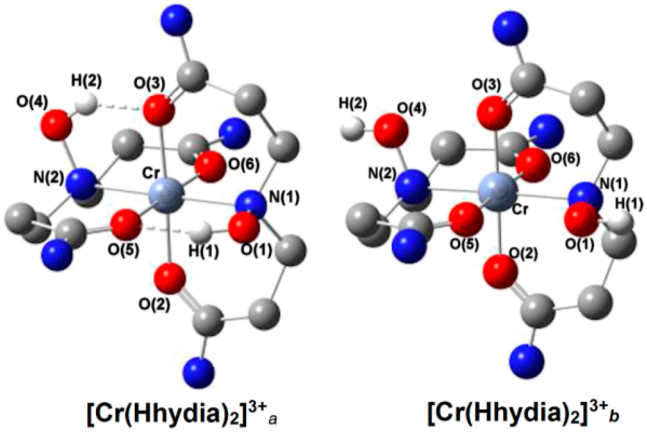

Figure 11. Optimized geometries of the complex $[Cr^{III}(Hhydia)_2]^{3+}$ {conformations $[Cr^{III}(Hhydia)_2]^{3+}{}_a$ and $[Cr^{III}(Hhydia)_2]^{3+}{}_b$} at the B3LYP level (hydrogen atoms except that of the hydoxylamine group are not shown for clarity).

Scheme 4

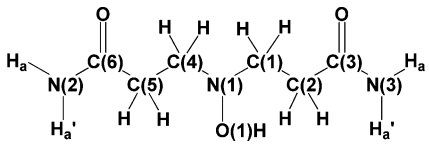

Scheme 5

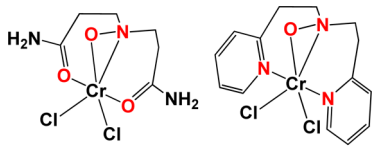

Scheme 6

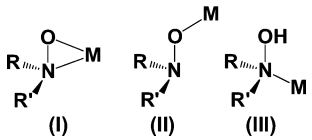

respectively) peaks indicating protonation of the hydroxylamine nitrogen atom. The large shift of the hydroxylamine proton, −OH, from 7.80 to 11.69 ppm also supports the protonation of the hydroxylamine nitrogen atom. All the ^{13}C NMR peaks of H_2hydia^+ Cl^- were shifted to higher field with the C(1) peak (Scheme 4) exhibiting the largest negative shift [-4.8 ppm compared to −2.3, −3.3 ppm for C(2) and C(3), respectively].

UV−vis Spectroscopy. The UV−vis spectrum of $\mathbf{1}\cdot H_2O$[29a] in methyl alcohol (Figure 4) gave one peak with a long tail on the right side of the spectrum at 521 (ε = 76.4 M^{-1} cm^{-1}) and one peak at 373 nm (ε = 97.9 M^{-1} cm^{-1}). The former peak was assigned to the lower energy d−d transition $^4T_2 \leftarrow {}^4A_2$, assuming O_h geometry. However, because the complex $\mathbf{1}\cdot H_2O$[29a] in the crystal structure has a slight tetragonal distortion, the T term should split to B_2 and E, and thus, the peak at 521 nm will be due to the sum of the $^4B_2 \leftarrow {}^4B_1$ and $^4E \leftarrow {}^4B_1$ transitions. However, the long tail indicates that the peak at 521 nm is the derivative of a more complex process, which was satisfactorily deconvoluted and fitted assuming the existence of two peaks of similar intensity located at 506 and 556 nm (Figure 4). The two peaks at 506 and 556 nm in the visible region of spectrum might be due to the distortion of the octahedral geometry of the complex $\mathbf{1}$[29b] or to the presence of two different chromium(III) species in the solution. Taking into account the high symmetry of $\mathbf{1}$[29b] (vide supra), such a large splitting is not justified.

The chromium(III) atom in $\mathbf{1}$[29b] occupies the center of an octahedral N_2O_4 coordination environment (vide supra), and thus, according to the Tanabe−Sugano diagram for octahedral complexes the $^4T_2 \leftarrow {}^4A_2$ (or more likely $^4B_2 + {}^4E \leftarrow {}^4B_1$ for the D_{4h} distortion) lowest energy transition equals to the Δ_o. The Δ_o values of the two species in the solution with peaks at 506 nm (1.98×10^4 cm^{-1}) and 556 nm (1.80×10^4 cm^{-1}) are compared very well with those calculated from the Jorgensen's equation ($\Delta_o = f\cdot g$). The calculated Δ_o values for octahedral chromium(III) species with a N_2O_4 and $Cl_2N_2O_2$ coordination environment are 525 nm (1.90×10^4 cm^{-1}) and 563 nm (1.78×10^4 cm^{-1}), respectively.[30] On the basis of this observation the peak at 506 nm was assigned to $\mathbf{1}$[29b], while the peak at 556 nm was assigned to the geometrical isomers *cis*-$[Cr^{III}Cl_2(Hhydia\text{-}N,O)_2]^+(\mathbf{2}_{cis})$ or *trans*-$[Cr^{III}Cl_2(Hhydia\text{-}N,O)_2]^+(\mathbf{2}_{trans})$ shown in Scheme 2 (vide supra).

The solid-state UV−vis diffuse reflectance spectrum of $\mathbf{1}\cdot H_2O$[29a] is similar to the spectrum of $\mathbf{1}\cdot H_2O$[29a] in solution (Figure 5) and consists of two major peaks located at 513 (1.95×10^4 cm^{-1}) and at 386 nm (2.59×10^4 cm^{-1}) and a shoulder at ~600 nm (1.67×10^4 cm^{-1}) assigned to the spin-allowed d−d transitions. In addition, the solid-state spectrum of $\mathbf{1}\cdot H_2O$[29a] gave also the weak spin-forbidden transition $^2E \leftarrow {}^4A_2$ (or more likely $^2A_1 + {}^2B_1 \leftarrow {}^4B_1$ for the D_{4h} distortion) at 695 nm (Figure 5). The peak at 513 and the shoulder at 560 nm reveal that even the complex of $\mathbf{1}\cdot H_2O$[29a] in the solid state (as prepared crystalline phase) is also a mixture of the isomers $\mathbf{1}$[29b] and **2** in agreement with the solution studies (vide supra).

dx.doi.org/10.1021/ic501778d | Inorg. Chem. 2014, 53, 11404−11414

The parameters B' and Δ_0 of **1**[29b] were calculated from the two spin-allowed (513 and 386 nm) and the spin-forbidden (695 nm) transitions (Figure 5, black line), using the d^3 Tanabe–Sugano diagram and were found to be 685 cm^{-1} and 1.95×10^4 cm^{-1}, respectively, which are very close to the values expected for an octahedral chromium(III) compound with a N_2O_4 coordination environment. The possibility of the formation of a chromium(III) complex with a Cr^{III}–NCO bond(s), that is, with the deprotonated amide(s) of the ligand Hhydia in solution was excluded because: (i) the p*K*a of the amide group is higher[31] than the hydroxylamine's proton, and thus, it is expected that the first deprotonation will be that of the hydroxylamine proton and then that of the amide; (ii) deprotonated amide donor groups are expected to shift the absorption peak[31] of the chromium(III) species in the UV–vis spectrum of it to more than 100 nm, and such a shift was not observed in either solid state or solution; and (iii) the solid-state and solution (CH_3OH) UV–vis spectra of **1**·H_2O are the same, and thus, they should contain similar species.

Aqueous solution of **1**·H_2O at the pH of dissolution (3.05) gave two peaks at 556 and 382 nm. These wavelengths were assigned to species **2** (vide supra), implying that **1** after its dissolution in water is converted immediately to isomers **2**. The spectrum of the aqueous solution of **1**·H_2O changes continuously with time. An overlay of the spectra of **1**·H_2O in aqueous solution at different times gave an isosbestic point at 530 nm (Supporting Information, Figure S7), revealing the formation of one new species that was not identified. At pH 7.18 the visible spectrum gave a broad peak at ~556 nm. The ligand decomposes relatively fast in these solutions, as this was revealed by the large absorption at wavelengths lower than 400 nm, which increase with time (vide infra).

Formation of the *cis*-[Cr^{III}(hydia)Cl_2] (3) in Solution. The possibility of formation of the neutral compound *cis*-[Cr^{III}(hydia)Cl_2] (**3**) in solution (Scheme 5) with a structure similar to the previously reported[32] Cr(III) complex with the *N*,*N*′-disubstituted hydroxylamine ligand Hbipyh, *cis*-[Cr^{III}(bipyh)Cl_2] (**4**), (Scheme 5), was also examined. For compound **3**, a peak at ~580 nm is predicted for the $^4A_2 \leftarrow {}^4T_2$ transition, assuming O_h symmetry d–d transition (however, the structure of complexes **3** and **4** exhibit approximately a C_{2v} symmetry, and thus, the peak at 580 nm will be due to $^4A_2+{}^4B_1+{}^4B_2 \leftarrow {}^4A_2$ transitions), using the UV–vis experimental data of **4** and the Jorgensen's equation to calculate the difference of the contribution of the two amide oxygen atoms versus the pyridine nitrogen atoms. The calculated value of 580 nm for the $^4A_2+{}^4B_1+{}^4B_2 \leftarrow {}^4A_2$ d–d transitions originating from **3** is significantly larger than the experimental maximum observed at 521 nm of the UV–vis spectrum of **1**·H_2O[29a] in solution (CH_3OH) suggesting that compound **3** does not exist in solution. This is also supported by theoretical calculations (see Supporting Information).

Real-Time Formation/Decomposition Studies of 1 in CH_3OH. The formation and decomposition of compound **1**[29b] was monitored by UV–vis spectroscopy (Figure 6) by mixing solutions of various concentrations of *trans*-[$Cr^{III}Cl_2(H_2O)_4$]-Cl·$2H_2O$ and the ligand Hhydia in methyl alcohol. The UV–vis spectra of these solutions as a function of the time gave two isosbestic points located at 634 and 455 nm during the first 2 min of the reaction. However, after the first 2 min the appearance of a new peak at 367 nm (Figure 6) and deviations from the isosbestic points indicate decomposition of the ligand. The logarithmic plot of the initial rates (k_{init}) versus various concentrations of chromium(III) or the ligand Hhydia (Supporting Information, Figure S7) revealed a first-order rate law toward the concentration of [Hhydia], and the observed rate constant at 25 °C was calculated to be 8.7(±0.8) $\times 10^{-5}$ M^{-1} s^{-1}. This rate constant falls within the range observed for the formation of chromium(III) compounds with ligands such as picolinic acid and amino acids. The fact that the rates for all these reactions are considerably faster, taking into account the Cr(III) kinetic inertness[33] and the corresponding water exchange reactions in chromium(III) species, has been attributed to an associative mechanism.[34]

However, the interference of the ligand decomposition in the complex formation is apparent from the UV–vis spectra. The decomposition of the ligand can be approximately estimated by the variation of the peak absorbance at 367 nm. The plot of the absorbance at 521 and 367 nm versus time (Supporting Information, Figure S8) for various concentrations of metal ion and ligand show similar variation at the first few minutes of the reaction depending on the concentration of the ligand. Then, at a time point that is reversibly analogous to the concentration of the ligand, the absorbance of the peak at 521 nm remains almost constant, whereas the peak at 367 nm continues to increase exponentially. The decomposition of the ligand versus time shows that it is probably a radical-mediated process (Supporting Information, Figure S7). Solutions of **1**·H_2O[29a] in CH_3OH of similar concentrations decompose much slower than the mixtures of metal with the ligand, showing stabilization of the ligand in the Cr(III) complex. This indicates that the decomposition of Hhydia is not due to the presence of the metal ions or the complex but rather to the nature of the free ligand. Indeed, the free ligand in solution (CH_3OH) decomposes even without the presence of chromium(III), as this was evidenced by UV–vis and ^1H NMR spectroscopies (Supporting Information, Figure S9). The redox activity of Hhydia and **1**·H_2O in MeOH was also examined by cyclic voltammetry (CV) (Supporting Information, Figure S10). Both voltamogramms gave two irreversible (one anodic and one cathodic) waves assigned to the reduction (ca. −0.2 V vs normal hydrogen electrode (NHE)) and oxidation (~1.0 V vs NHE) of the hydroxylamine group.

Magnetism and Electron Paramagnetic Spectra (EPR). The magnetic moment of the chromium(III)-Hhydia solids isolated from either ethyl alcohol or isopropyl alcohol and from methyl alcohol/diethyl ether (the crystalline material) was found to be 3.80 μ_B, as expected for a d^3 system.[35] The EPR spectrum of **1**·H_2O[29a] in CH_3OH gave three peaks at g = 4.0, 2.0, and 1.2, thus indicating a system with moderately large zero-field splitting and small rhombicity. However, the simulation of the spectrum using the Hamiltonian in eq 1 showed that the experimental line shape cannot be reproduced by a single S = 3/2 species with a well-defined value for E/D.

$$H = D\left[S_z^2 - \frac{1}{3}S(S+1)\right] + E(S_x^2 - S_y^2) + g_z\mu_B H_z S_z + g_x\mu_B H_x S_x + g_y\mu_B H_y S_y \quad (1)$$

The spectrum was better simulated applying two components, one fully rhombic [g = 1.97, D = 8312 MHz (0.277 cm^{-1}), E = 2658 MHz (0.0887 cm^{-1}), E/D = 0.32] assigned to the crystallographically characterized complex **1**,[29b] and one axial [g = 1.97, D = 11718 MHz (0.391 cm^{-1}), E = 1.88 MHz (0.006 cm^{-1}), E/D = 0.05] in 55:45 ratio (Figure 7).

dx.doi.org/10.1021/ic501778d | *Inorg. Chem.* 2014, 53, 11404–11414

The X-band powder EPR spectrum of $1\cdot H_2O$[29a] gave peaks at $g \approx 4.9$, 3.6, 2.5, 2.0, 1.5, and 1.2 (Figure 8). The very strong peak at $g = 4.9$ indicates a system with a rhombic character and a large D value. However, the number and position of the rest of the peaks do not fit with any E/D ratio of the rhombogramm for $S = 3/2$. The presence of more than one chromium(III) species was confirmed by the spectra of solids isolated from interaction of Hhydia with *trans*-$[Cr^{III}Cl_2(H_2O)_4]Cl\cdot 2H_2O$ in C_2H_5OH and $(CH_3)_2CHOH$. In particular the peak at $g = 2.0$ shows a higher intensity for the solid isolated from $(CH_3)_2CHOH$ than it does from C_2H_5OH or $CH_3OH/(C_2H_5)_2O$.

A reasonable fitting of the spectrum of $1\cdot H_2O$[29a] was successful using two different anisotropic systems with $g_{//} = 1.957$, $g_{\perp} = 1.987$, $D = 7952$ MHz (0.265 cm^{-1}), $E = 1736$ MHz (0.0579 cm^{-1}), $E/D = 0.22$ (weight 30%) and $g_{//} = 1.956$, $g_{\perp} = 1.987$, $D = 9414$ MHz (0.314 cm^{-1}), $E = 3006$ MHz (0.100 cm^{-1}), $E/D = 0.32$ (weight 70%) (Figure 8). The more abundant component in solid state was assigned to complex **1**.[29b]

Both solution and solid-state EPR data and the UV−vis (solution and solid state) spectra of $1\cdot H_2O$ are in agreement showing the presence of the isomers **1** and **2** in solid state and in solution.[29a]

Conductivity. To further confirm the assignment of the various Cr^{III}−Hhydia species in solution to "ionization isomers", the conductivity of the solid isolated from the interaction of Hhydia with *trans*-$[Cr^{III}Cl_2(H_2O)_4]Cl\cdot 2H_2O$ in either C_2H_5OH or $(CH_3)_2CHOH$ and $CH_3OH/(C_2H_5)_2O$ was measured in methyl alcohol, and it was found in the range of 189−203 cm^{-1} mol^{-1} Ω^{-1}. This range of conductivity values corresponds to a species with three ions and/or a mixture of **1**[29b] (four ions) and **2** (two ions) formed in solution. The presence of a mixture of **1** and **2** in MeOH solution is in agreement with the spectroscopic characterization (vide supra, EPR, and UV−vis) and the ESI-MS (vide infra) of the solution.

ESI-MS Studies. ESI-MS studies of the $[Cr^{III}(Hhydia)_2]Cl_3\cdot H_2O$ ($1\cdot H_2O$[29a]) dissolved in methyl alcohol confirmed that the compound retained its integrity in solution (Figure 9) during the course of the MS studies. The observed distribution envelopes were assigned to the singly charged species $\{[Cr^{III}(hydia)_2]\}^+$, $[\mathbf{1}\text{-}2H/3Cl]^+$ and/or $[\mathbf{2}\text{-}2HCl]$, $\{[Cr^{III}(Hhydia)(hydia)Cl\}^+$, $[\mathbf{2}\text{-}HCl]^+$ and/or $[\mathbf{1}\text{-}H/2Cl]$, and $\{[Cr^{III}(Hhydia)_2Cl_2]\}^+$ centered at m/z ca. 400.04, 436.02, and 472.07, respectively. The loss of the N−OH proton takes place in some species during the course of the ESI-MS studies. This type of phenomena such as change of the redox state of the transition metal center and gain or loss of protons and/or solvent molecules is something quite common and has been observed before.[36] The ESI-MS investigation has given us additional information in regard to the speciation of the complex $1\cdot H_2O$[29a] in solution. Unfortunately, consideration of the ESI-MS data as the sole source of evidence cannot give in this case unambiguous proof of the existence of specific isomers in solution. Nevertheless, this set of data is definitely additional supporting evidence only in combination with the data obtained from UV−vis, EPR, conductivity, and DFT calculations.

THEORETICAL STUDY

Molecular Structures of Compounds Hhydia, 1, and 2. The optimized molecular structures of two conformers of the ligand Hhydia, namely, $[Hhydia]_a$ and $[Hhydia]_b$, and its deprotonated form, $[hydia]^-$, at the B3LYP level, all adopting a C_s symmetry, are shown in Figure 10, whereas selected calculated and experimental {in the case of $[Hhydia]_a$} bond lengths are given in Supporting Information, Table S6. The most stable conformation of the ligand, $[Hhydia]_a$, is very close to the experimental one determined by X-ray structure analysis, whereas the second conformer of the ligand, $[Hhydia]_b$, adopting the geometry found in the complex $[Cr^{III}(Hhydia)_2]^{3+}$, is located only 6.7 kJ/mol higher in energy. The deprotonated form of the ligand, $[hydia]^-$, is stabilized by two strong hydrogen bonds between two hydrogen atoms (one from each H_2N_{amide} group) and the deprotonated hydroxylamine oxygen atom (Figure 10). The deprotonation of the two conformers $[Hhydia]_a$ and $[Hhydia]_b$ is endothermic by 1427 and 1420 kJ/mol, respectively.

The optimized molecular structure of the cation $[Cr^{III}(Hhydia)_2]^{3+}$ of complex **1**, at the B3LYP level, is shown as $[Cr^{III}(Hhydia)_2]^{3+}{}_a$ in Figure 11, whereas selected calculated and experimental bond lengths and angles are given in Supporting Information, Table S7. The calculated and experimental geometrical parameters of the $[Cr^{III}(Hhydia)_2]^{3+}$ complex are found to be in good agreement. The ligand Hhydia in **1** acts as a tridentate *O,N,O*-donor and adopts a C_2 symmetry. Its hydroxylamine group remains protonated and binds to the chromium(III) atom through the nitrogen of the N−OH unit (Scheme 6, III), while the oxygen atom is located at the nonbonding distance of ∼3 Å.

The octahedral structure of the $[Cr^{III}(Hhydia)_2]^{3+}$cation is further stabilized by two intramolecular hydrogen bonds between the hydrogen atom attached to $O_{hydroxylamine}$ of one ligand and the carbonyl oxygen atom of the other and vice versa (Figure 10, conformation $[Cr^{III}(Hhydia)_2]^{3+}{}_a$). A reoptimization of the complex $[Cr^{III}(Hhydia)_2]^{3+}$, starting from an initial structure where the two hydrogen atoms of the hydroxylamine groups were rotated away from the carbonyl oxygen atoms, gave a structure with no hydrogen bonds, which is a local minimum in the potential energy surface of the molecule. The latter structure, shown as $[Cr^{III}(Hhydia)_2]^{3+}{}_b$ in Figure 11, is located 14 kJ/mol higher in energy in comparison with the structure of $[Cr^{III}(Hhydia)_2]^{3+}{}_a$, and this gives a crude estimation of the stabilization energy being 7.1 kJ/mol for each hydrogen bond. Selected bond lengths and angles calculated for $[Cr^{III}(Hhydia)_2]^{3+}{}_b$ are given in Supporting Information, Table S7.

The optimized structures of the dichloro-*cis*/*trans*-$[Cr^{III}Cl_2(Hhydia\text{-}N,O)_2]^+$ species have C_1 symmetry and are shown in Figure 12, whereas their selected calculated bond lengths and angles are given in Supporting Information, Table S8. The compounds *cis*/*trans*-$[Cr^{III}Cl_2(Hhydia\text{-}N,O)_2]^+$ Cl^- and $[Cr^{III}(Hhydia\text{-}O,N,O)_2]^{3+}Cl^-{}_3$ (**1**) may be considered as ionization isomers. The *trans*-isomer was found to be more stable than the *cis*-isomer by 80.8 kJ/mol. In the *cis*/*trans*-$[Cr^{III}Cl_2(Hhydia\text{-}N,O)_2]^+$ isomers both Hhydia ligands act as chelating *N,O*-bidentate ones through the hydroxylamine nitrogen and the amide oxygen atoms. In the *cis*-isomer there are two hydrogen bonds; the hydroxylamine hydrogen of one Hhydia ligand is H-bonded to the amide oxygen of the second Hhydia ligand (N−O−H···O), and the hydroxylamine hydrogen of the second Hhydia ligand is H-bonded to the coordinated chlorine atom (N−O−H···Cl) (Figure 12). In the *trans*-isomer both hydroxylamine hydrogen atoms are H-bonded with the two *trans*-chlorine atoms (N−O−H···Cl) (Figure 12).

dx.doi.org/10.1021/ic501778d | Inorg. Chem. 2014, 53, 11404−11414

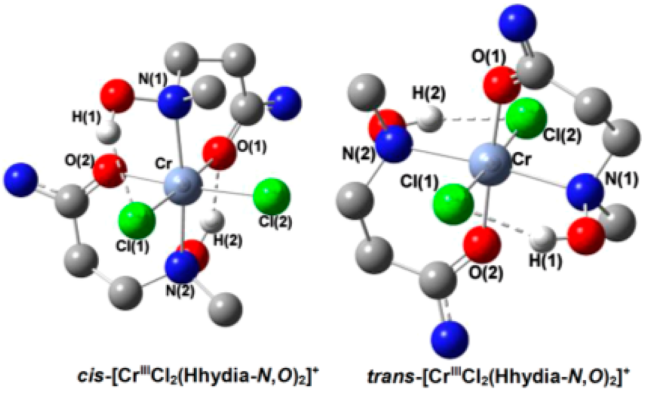

Figure 12. Optimized geometries of the *cis*/*trans*-$[Cr^{III}Cl_2(Hhydia)_2]^+$ isomers at the B3LYP level.

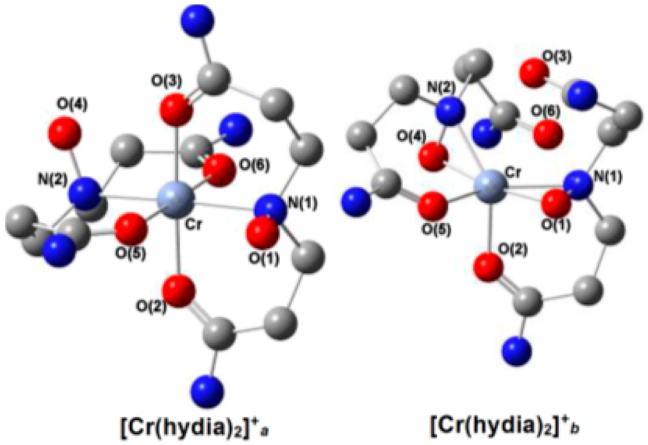

Figure 13. Optimized geometries of the complex $[Cr^{III}(hydia)_2]^+$ {topomers $[Cr^{III}(hydia)_2]^+_a$ and $[Cr^{III}(hydia)_2]^+_b$} at the B3LYP level (hydrogen atoms except that of the hydoxylamine group are not shown for clarity).

A reoptimization of the *cis*/*trans*-$[Cr^{III}Cl_2(Hhydia\text{-}N,O)_2]^+$ isomers starting from initial structures where one or two of the H-bonded hydrogen atoms are rotated away from H-acceptors gave a crude estimation of the stabilization energy for hydrogen bonds as follows: *cis*-isomer; (N−O−H···O) 21 kJ/mol, (N−O−H···Cl) 44 kJ/mol, *trans*-isomer; 2 × (N−O−H···Cl) 104 kJ/mol and consequently are considered as moderate strength H-bonds.[37,38] Nevertheless, in the non-H-bonded structures the *trans*-conformer is more favorable than the *cis*-conformer by 42.3 kJ/mol. The relative stability of both isomers is also confirmed by the higher adiabatic interaction energy between the $[Cr^{III}Cl_2]^+$ metal fragment with the two Hhydia ligands being 1026 and 969 kJ/mol for the *trans*- and *cis*-isomers, respectively.

Stability of $[Cr^{III}(hydia)_2]^+$ Species Containing Deprotonated Hydroxylamine Groups. The unmodified hydroxylamine (R = R′ = H), the *N*-substituted (R = H, R′ = alkyl), and the *N*,*N*′-disubstituted hydroxylamines exhibit three types of metal binding (Scheme 6). They can bind either in a side-on fashion (Type I) or *O*-bound (Type II)[14,19] with deprotonation of the hydroxyl group and as *N*-bound with the hydroxyl group not participating in metal coordination (Type III). In our study the complex $[Cr^{III}(Hhydia)_2]^{3+}$ exhibits Type III metal binding.

To investigate the mode of metal binding of the deprotonated hydia$^-$ ligand, a series of calculations were done for $[Cr^{III}(hydia)_2]^+$. Two stable topomers, namely, $[Cr^{III}(hydia)_2]^+_a$ and $[Cr^{III}(hydia)_2]^+_b$, were found as real minima in the potential energy surface. Both have a C_2 symmetry, and their optimized structures are shown in Figure 13, whereas their selected calculated bond lengths and angles are given in Supporting Information, Table S7. In the most stable structure, $[Cr^{III}(hydia)_2]^+_a$, the chromium(III) atom has an octahedral geometry very close to that found in $[Cr^{III}(Hhydia)_2]^{3+}$, which was characterized by X-ray structural analysis (Figure 2). The two deprotonated ligands hydia$^-$ in the $[Cr^{III}(hydia)_2]^+_a$ bind also through the nitrogen atom of N−O$^-$ functionality, although a weak interaction between Cr and $O^-_{hydroxylamine}$ should not be excluded due to the shortening of the Cr···O distance 2.847 Å (the predicted Cr···OH distance in $[Cr^{III}(Hhydia)_2]^{3+}$ is 3.006 Å). The second topomer, $[Cr^{III}(hydia)_2]^+_b$, has a highly deformed structure with the hydroxylamine N−O$^-$ functionalities binding in a side-on mode and is located 108 kJ/mol higher in energy than $[Cr^{III}(hydia)_2]^+_a$. The deprotonation of the two N−OH groups of $[Cr^{III}(Hhydia)_2]^{3+}_a$ leads to two topomers, $[Cr^{III}(hydia)_2]^+_a$ and $[Cr^{III}(hydia)_2]^+_b$, and is endothermic by 1414 and 1306 kJ/mol, respectively. Thus, the experimental isolation of the complex cation $[Cr^{III}(hydia)_2]^+$ seems energetically unfavorable due to both the instability of both topomers of $[Cr^{III}(hydia)_2]^+$ as well as the stabilization of $[Cr^{III}(Hhydia)_2]^{3+}_a$ coming from the intramolecular hydrogen bonds already described {vide supra in the crystal structure description of $[Cr^{III}(Hhydia)_2]^{3+}$}.

CONCLUSIONS

In this paper, the interaction of the biologically relevant ligand 3,3′-(hydroxyazanediyl)dipropanamide (Hhydia) with chromium(III) was investigated by means of X-ray structural analysis, UV−vis, EPR, MS, and IR spectroscopy and DFT calculations. The deprotonation of the hydroxylamine group of the ligand Hhydia does not take place in the complex $[Cr^{III}(Hhydia)_2]Cl_3$ in marked contrast to what somebody would expect on the basis of the oxidation state III of the chromium and the only other reported example of a Cr^{III}-*N*,*N*′-disubstituted hydroxylamine compound[32] in which the hydroxylamine group is deprotonated.

Since chromium(III) in the complex $[Cr^{III}(Hhydia)_2]Cl_3$ does not deprotonate the hydroxylamine proton, which has a much lower pK_a value in comparison with the amidic protons, this means that the most probable site of interaction of it with peptides or proteins in the biological systems is the amidic oxygen. The X-ray structural analysis of the complex $[Cr^{III}(Hhydia\text{-}O,N,O)_2]^{3+}$ provides an evidence in solid state that the Cr(III)−O_{amide} binding is a possible mode of interaction in peptides and proteins.

UV−vis and EPR studies, both in solution and in the solid state, ESI-MS, and conductivity measurements support the fact that irrespective of the solvent used in the interaction of Hhydia with *trans*-$[Cr^{III}Cl_2(H_2O)_4]Cl{\cdot}2H_2O$ yields the ionization isomers $[Cr^{III}(Hhydia)_2]Cl_3{\cdot}2H_2O$ (**1**·$2H_2O$) and *cis*/*trans*-$[Cr^{III}Cl_2(Hhydia)_2]Cl{\cdot}2H_2O$ (**2**·$2H_2O$). DFT calculations support the thermodynamic stability of all the ionization isomers. The *cis*/*trans*-$[Cr^{III}(Hhydia)_2Cl_2]Cl$ species might be considered as a thermodynamically stable first adduct of the reaction of *trans*-$[Cr^{III}Cl_2(H_2O)_4]Cl{\cdot}2H_2O$ with Hhydia, disclosing a possible pathway toward the formation of $[Cr^{III}(Hhydia)_2]Cl_3$. The reaction rate constant of the formation of the Cr(III) complexes **1**·$2H_2O$ and **2**·$2H_2O$ with the ligand Hhydia was found to be $8.7(\pm0.8) \times 10^{-5}$ M^{-1}

dx.doi.org/10.1021/ic501778d | *Inorg. Chem.* 2014, 53, 11404−11414

s^{-1}. Such a reaction rate constant is considerably faster in comparison with the corresponding water exchange rate constant for the hydrated chromium(III). The modification of the kinetics is of fundamental importance for the chromium(III) chemistry in biological systems.

■ ASSOCIATED CONTENT

Supporting Information

Experimental details for physicochemical measurements, computational discussion, that is, comparison of the stability of *cis*-[$Cr^{III}Cl_2$(hydia)] with *cis*-[Cr^{III}(bipyh)Cl_2], vibrational spectra of compounds Hhydia and **1**, NMR spectra, cyclic voltammogram, structural drawings, tabulated crystallographic and NMR data. X-ray crystallographic files in CIF format for the structures of compounds Hhydia and **1**·H_2O. This material is available free of charge via the Internet at http://pubs.acs.org.

■ AUTHOR INFORMATION

Corresponding Authors

*E-mail: harism@chem.gla.ac.uk. (H.N.M.)
*E-mail: sigalas@chem.auth.gr. (M.P.S.)
*E-mail: akeramid@ucy.ac.cy. (A.D.K.)
*E-mail: tkampano@cc.uoi.gr. (T.A.K.)

Notes

The authors declare no competing financial interest.

■ ACKNOWLEDGMENTS

We are grateful to the Greek Community Support Framework III, Regional Operational Program of Epirus 2000-2006 (MIS 91629), for supporting the purchase of the LC-NMR cryo instrument. The authors would like to thank the Unit of Environmental, Organic and Biochemical high resolution analysis-ORBITRAP-LC-MS of the University of Ioannina for providing access to the facilities. We also thank the Research Promotional Foundation of Cyprus and the European Structural Funds for the purchase of EPR through ΑΝΑΒΑΘΜΙΣΗ/ΠΑΓΙΟ/0308/32 and Dr. C. Drouza for the EPR measurements. Also we would like to thank the Univ. of Glasgow, WestCHEM, and Prof. L. Cronin for providing access to the X-ray and ESI-MS facilities.

■ REFERENCES

(1) Ding, Y.; Ji, Z. *Production and Application of Chromium Compounds;* Chemical Industry Press: Beijing, 2003.

(2) (a) Lansdown, A. B. G. *The Carcinogenicity of Metals: Human risk through occupational and environmental exposure;* Royal Society of Chemistry: London, 2014; pp 53−75. (b) Sarkar, B. *Metallomics* **2012**, *4*, 589−592. (c) Parkin, D. M. *Br. J. Cancer* **2011**, *105*, S70−S72.

(3) Shi, X.; Dalal, N. S. *Biochem. Biophys. Res. Commun.* **1988**, *156*, 137−152.

(4) (1) (a) Judah, L.; Marin, R.; Stroup, D.; Wesdemiotis, C.; Bose, R. N. *Toxicol. Res.* **2014**, *3*, 56−66. (b) Marin, R.; Ahuja, Y.; Jackson, G. P.; Laskay, U.; Bose, R. N. *J. Am. Chem. Soc.* **2011**, *133*, 17519−17519. (c) Marin, R.; Ahuja, R.; Bose, R. N. *J. Am. Chem. Soc.* **2010**, *132*, 10617−10619.

(5) (a) Bartholomaus, R.; Irwin, J. A.; Shi, L.; Smith, S. M.; Levina, A.; Lay, P. A. *Inorg. Chem.* **2013**, *52*, 4282−4292. (b) Bartholomaus, R.; Harms, K.; Levina, A.; Lay, P. A. *Inorg. Chem.* **2012**, *51*, 11238−11240. (c) Levina, A.; Zhang, L.; Lay, P. A. *J. Am. Chem. Soc.* **2010**, *132*, 8720−8731. (d) Lay, P. A.; Levina, A. *J. Am. Chem. Soc.* **1998**, *120*, 6704−6714. (e) Farrell, R. P.; Judd, R. J.; Lay, P. A.; Dixon, N. E.; Baker, R. S. U.; Bonin, A. M. *Chem. Res. Toxicol.* **1989**, *2*, 227−229. (f) Barr-David, G.; Hambley, T. W.; Irwin, J. A.; Judd, R. J.; Lay, P. A.; Martin, B. D.; Bramley, R.; Dixon, N. E.; Hendry, P.; Ji, J.-Y.; Baker, R. S. U.; Bonin, A. M. *Inorg. Chem.* **1992**, *31*, 4906−4908. (g) Dillon, C. T.; Lay, P. A.; Bonin, A. M.; Cholewa, M.; Legge, G. J. F.; Collins, T. J.; Kostka, K. L. *Chem. Res. Toxicol.* **1998**, *11*, 119−129.

(6) (a) Flora, D. D.; Wetterhahn, K. E. *Life Chem. Rep.* **1989**, *7*, 169−244. (b) Bose, R. N.; Moghaddas, S.; Gelerinter, E. *Inorg. Chem.* **1992**, *31*, 1987−1994. (c) Moghaddas, S.; Gelerinter, E.; Bose, R. N. *J. Inorg. Biochem.* **1995**, *57*, 135−146.

(7) (a) Reynolds, M.; Armknecht, S.; Johnston, T.; Zhitkovich, A. *Mutagenesis* **2012**, *27*, 437−443. (b) Shi, X.; Mao, Y.; Knapton, A. D.; Ding, M.; Rojanasakul, Y.; Gannett, P. M.; Dalai, N.; Liu, K. *Carcinogenesis* **1994**, *15*, 2475−2478.

(8) Cupo, D. Y.; Wetterhahn, K. E. *Proc. Natl. Acad. Sci. U. S. A.* **1985**, *82*, 6755−6759.

(9) (a) Aviva Levina, A.; Lay, P. A. *Chem. Res. Toxicol.* **2008**, *21*, 563−571. (b) Levina, A.; Lay, P. A. *Coord. Chem. Rev.* **2005**, *249*, 281−298. (c) Levina, A.; Mulyani, I.; Lay, P. A. In *The Nutritional Biochemistry of Chromium(III);* Vincent, J., Ed.; Elsevier: Amsterdam, 2007; pp 225−256. (d) Mulyani, I.; Levina, A.; Lay, P. A. *Angew. Chem., Int. Ed.* **2004**, *43*, 4504−4507. (e) Lay, P. A.; Levina, A. In *Encyclopedia of Inorganic and Bioinorganic Chemistry;* Scott, R. A., Ed.; John Wiley & Sons: Chichester, U.K., 2012; DOI: 10.1002/9781119951438.eibc0040.pub2.

(10) (a) Vincent, J. B. *Dalton Trans.* **2010**, *39*, 3787−3794. (b) *The Bioinorganic Chemistry of Chromium;* Vincent, J. B., Ed.; John Wiley & Sons Ltd: Chichester, U.K., 2013.

(11) (a) Hepburn, D. D. D.; Vincent, J. B. *Chem. Res. Toxicol.* **2002**, *15*, 93−100. (b) Al-Qatati, A.; Winter, P. W.; Wolf-Ringwall, A. L.; Chatterjee, P. B.; Van Orden, A. K.; Crans, D. C.; Roess, D. A.; Barisas, B. G. *Cell Biochem. Biophys.* **2012**, *62*, 441−450 and references therein.

(12) (a) Speetjens, J. K.; Collins, R. A.; Vincent, J. B.; Woski, S. A. *Chem. Res. Toxicol.* **1999**, *12*, 483−487. (b) Hepburn, D. D. D.; Burney, J. M.; Woski, S. A.; Vincent, J. B. *Polyhedron* **2003**, *22*, 455−463. (c) Cefalu, W. T.; Hu, F. B. *Diabetes Care* **2004**, *27*, 2741−2751. (d) Coryell, V. H.; Stearns, D. M. *Mutat. Res., Genet. Toxicol. Environ. Mutagen.* **2006**, *610*, 114−123. (e) Vincent, J. B. *Dalton Trans.* **2010**, *39*, 3787−3794. (f) Levina, A.; Lay, P. A. *Dalton Trans.* **2011**, *40*, 11675−11686.

(13) (a) Murdoch, C. M.; Cooper, M. K.; Hambley, T. W.; Hunter, W. N.; Freeman, H. C. *J. Chem. Soc., Chem. Commun.* **1986**, 1329−133. (b) Tkaczyk, C.; Huk, O. L.; Mwale, F.; Antoniou, J.; Zukor, D. J.; Petit, A.; Tabrizian, M. *J. Biomed. Mater. Res., Part A* **2010**, *94*, 214−222. (c) Mizuochi, H.; Uehara, A.; Kyono, E.; Tsuchida, R. *Bull. Chem. Soc. Jpn.* **1971**, *77*, 5482. (d) Gillard, R. D.; Laurie, S. H.; Price, D. C.; Phipps, D. A.; Weick, C. F. *J. Chem. Soc., Dalton Trans.* **1974**, 1385. (e) Oki, H.; Takahash, Y. *Bull. Chem. Soc. Jpn.* **1977**, *50*, 2280. (f) Oki, H.; Otsuka, K. *J. Sci. Hiroshima Univ.* **1982**, *45A*, 463.

(14) (a) Nikolakis, V. A.; Tsalavoutis, J. T.; Stylianou, M.; Evgeniou, E.; Jakusch, T.; Melman, A.; Sigalas, M. P.; Kiss, T.; Keramidas, A. D.; Kabanos, T. A. *Inorg. Chem.* **2008**, *47*, 11698−11710. (b) Nikolakis, V. A.; Exarchou, V.; Jakusch, T.; Woolins, J. D.; Slawin, A. M. Z.; Kiss, T.; Kabanos, T. A. *Dalton Trans.* **2010**, *39*, 9032−9038. (c) Nikolakis, V. A.; Stathopoulos, P.; Exarchou, V.; Gallos, J. K.; Kubicki, M.; Kabanos, T. A. *Inorg. Chem.* **2010**, *49*, 52−61. (d) Stylianou, M.; Nikolakis, V. A.; Chilas, G. I.; Jakusch, T.; Vaimakis, T.; Kiss, T.; Sigalas, M. P.; Keramidas, A. D.; Kabanos, T. A. *Inorg. Chem.* **2012**, *51*, 13138−13147.

(15) (a) *Bioinorganic Vanadium Chemistry;* Rehder, D., Ed.; John Wiley& Sons Ltd: West Sussex, England, 2008. (b) Li, C.; Oberlies, N. H. *Life Sci.* **2005**, *78*, 532−538. (c) Garner, C. D.; Armstrong, E. M.; Berry, R. E.; Beddoes, R. L.; Collison, D.; Cooney, J. J. A.; Ertok, S. N.; Helliwell, M. *J. Inorg. Biochem.* **2000**, *80*, 17−20. (d) Armstrong, E. M.; Beddoes, R. L.; Calviou, L. J.; Charnock, J. M.; Collison, D.; Ertok, N.; Naismith, J. H.; Garner, C. D. *J. Am. Chem. Soc.* **1993**, *115*, 807−808. (e) Armstrong, E. M.; Collison, D.; Ertok, N.; Garner, C. D. *Talanta* **2000**, *53*, 75−87. (f) Berry, R. E.; Armstrong, E. M.; Beddoes, R. L.; Collison, D.; Ertok, S. N.; Helliwell, M.; Garner, C. D. *Angew. Chem., Int. Ed. Engl.* **1999**, *38*, 795−797. (g) Smith, P. D.; Berry, R. E.; Harben, S. M.; Beddoes, R. L.; Helliwell, M.; Collison, D.; Garner, C. D. *J. Chem. Soc., Dalton Trans.* **1997**, *23*, 4509−4516. (h) Da Silva, J.

A.L.; Da Silva, J. J.R.; Pombeiro, A. J. L. *Coord. Chem. Rev.* **2013**, *257*, 2388−2400.
(16) Wencewicz, T. A.; Yang, B.; Rudloff, J. R.; Oliver, A. G.; Miller, M. J. *J. Med. Chem.* **2011**, *54*, 6843−6858.
(17) (a) Ohkatsu, Y.; Baba, R.; Watanabe, K. *J. Jpn. Pet. Inst.* **2011**, *54*, 15−21. (b) Trnka, J.; Blaikie, F. H.; Logan, A.; Smith, R. A. J.; Murphy, M. P. *Free Radical Res.* **2009**, *43*, 4−12.
(18) Miller, R. R.; Doss, G. A.; Stearns, R. A. *Drug Metab. Dispos.* **2003**, *32*, 178−185.
(19) (a) Gun, J.; Ekeltchik, I.; Lev, O.; Shelkov, R.; Melman, A. *Chem. Commun.* **2005**, 5319−5321. (b) Ekeltchik, I.; Gun, J.; Lev, O.; Shelkov, R.; Melman, A. *Dalton Trans.* **2006**, 1285−1293. (c) Peri, D.; Alexander, J. S.; Tshuva, E. Y.; Melman, A. *Dalton Trans.* **2006**, 4169−4172. (d) Shavit, M.; Peri, D.; Melman, A.; Tshuva, E. Y. *J. Biol. Inorg. Chem.* **2007**, *12*, 825−830. (e) Melman, G.; Vimal, P.; Melman, A. *Inorg. Chem.* **2009**, *48*, 8662−8664. (f) Bou-Abdallah, F.; McNally, J.; Liu, X. X.; Melman, A. *Chem. Commun.* **2011**, 731−733.
(20) Kimura, T.; Kato, E.; Machikava, T.; Kimura, S.; Katayama, S.; Kawabata, J. *Biochem. Biophys. Res. Commun.* **2014**, *445*, 6−9.
(21) Willsky, G. R.; Chi, L.-H.; Godzala, M.; Kostyniak, P. J.; Smee, J. J.; Trujillo, A. M.; Alfano, J. A.; Dinb, W.; Hu, Z.; Crans, D. C. *Coord. Chem. Rev.* **2011**, *255*, 2258−2269.
(22) Klemchuk, P.; US3818006; 1974, *81*, nb.105575.
(23) (a) Dey, A.; Lakshmanan. *J. Funct. Foods* **2013**, *4*, 1148−1184. and references therein. (b) Mari, M.; Colell, A.; Morales, A.; von Montfort, C.; Garcia-Ruiz, C.; Fernandez-Checa, J. C. *Antioxid. Redox Signaling* **2010**, *12*, 1295−1331. (c) Reuter, S.; Gupta, S. C.; Chaturvedi, M.; Aggarwal, B. B. *Free Radical Biol. Med.* **2010**, *49*, 1603−1616.
(24) (a) Lee, Y. P.; Kim, D. W.; Kang, H. W.; Hwang, J. H.; Jeong, H. J.; Sohn, E. J.; Kim, M. J.; Ahn, E. H.; Shin, M. J.; Kim, D. S.; Kang, T. C.; Kwon, O. S.; Cho, S. W.; Park, J.; Eum, W. S.; Choi, S. Y. *FEBS J.* **2012**, *279*, 1929−1942. (b) Al-Maskari, M. Y.; Waly, M. I.; Ali, A.; Al-Shuaibi, Y. S.; Ouhtit, A. *Nutrition* **2012**, *28*, e23−e26. (c) Deo, S. H.; Fisher, J. P.; Vianna, L. C.; Kim, A.; Chockalingam, A.; Zimmerman, M. C.; Zucker, I. H.; Fadel, P. J. *Am. J. Physiol.: Heart Circ. Physiol.* **2012**, *303*, H377−H385. (d) Sanchez-Valle, V.; Chavez-Tapia, N. C.; Uribe, M.; Mendez-Sanchez, N. *Curr. Med. Chem.* **2012**, *19*, 4850−4860. (e) Eskici, G.; Axelsen, P. H. *Biochemistry* **2012**, *51*, 6289−6311. (f) Barberger-Gateau, P.; Lambert, J. C.; Feart, C.; Peres, K.; Ritchie, K.; Dartigues, J. F.; Alperovitch, A. *J. Alzheimer's Dis.* **2012**, *33*, S457−S463.
(25) *CRC Handbook of Chemistry and Physics*, 76th ed.; CRC Press: Boca Raton, FL, 1995.
(26) Tandford, C. *Adv. Protein Chem.* **1962**, *17*, 69−165.
(27) Wang, D.; Liu, S.; Zeng, Y.; Sun, W.-H.; Redshaw, C. *Organometallics* **2011**, *30*, 3001−3009.
(28) Trigonal prism, $q = 0°$; octahedron, $q = 60°$. Huheey, J. E.; Keiter, E. A.; Keiter, R. L. In *Inorganic Chemistry: Principles of Structure and Reactivity;* 4th ed.; HarperCollins College Publishers: New York, 1993; p 490.
(29) (a) In all solution and solid-state measurements, the crystalline material used was isolated from the reaction of Hhydia with *trans*-$[Cr^{III}Cl_2(H_2O)_4]Cl{\cdot}2H_2O$ in methyl alcohol/diethyl ether, and it is abbreviated as $\mathbf{1}{\cdot}H_2O$, although it has been proved from UV−vis, EPR, MS, and conductivity measurements to be a mixture of the ionization isomers $[Cr^{III}(Hhydia)_2]Cl_3$ (**1**, ∼70%) and *cis/trans*-$[Cr^{III}Cl_2(Hhydia)_2]Cl{\cdot}2H_2O$ ($\mathbf{2}_{cis/trans}$, ∼30%). (b) **1** is used to denote the crystallographically characterized chromium(III) compound $[Cr^{III}(Hhydia)_2]Cl_3$.
(30) The value of g for Cr(III) equals to 17 400 cm^{-1}; the value of f for chlorine, nitrogen, and oxygen atoms equals to 0.78, 1.28, and 1.00, respectively.
(31) Daeid, N. N.; Nolan, K. B.; Ryan, L. P. *J. Chem. Soc., Dalton Trans.* **1991**, 2301−2304.
(32) Belock, C. W.; Cetin, A.; Barone, N. V.; Ziegler, C. J. *Inorg. Chem.* **2008**, *47*, 7114−7120.
(33) Lay, P. A.; Levina, A. *Comprehensive Coordination Chemistry II: From Biology to Nanotechnology;* McCleverty, J. A., Meyer, T. J., Eds.; Elsevier: Amsterdam, 2004, Vol. *4*, pp 313−413.
(34) (a) Burgress, J.; Hubbard, C. D. In *Advances in Inorganic Chemistry;* van Eldik, R., Eds.; Elsevier: Amsterdam, 2003, *54*, pp 72−140. (b) Guindy, N. M.; Abou-Gamra, Z. M.; Abdel-Messih, M. F. *Monatsh. Chem.* **2000**, *131*, 857−866.
(35) The X_{Di} of the Cl^- as counteranion is -23.4×10^{-6} emu mol^{-1}, and it is similar to the value of 22.6 emu mol^{-1} for the ligated chlorine atom to a metal atom ($X_{Di} = -20.1 \times 10^{-6}$ emu mol^{-1} plus -2.5×10^{-6} emu mol^{-1} of the contribution of the covalent bond). Thus, the total diamagnetic corrections are very similar for all the ionization isomers.
(36) (a) Miras, H. N.; Wilson, E. F.; Cronin, L. *Chem. Commun.* **2009**, 1297−1311. (b) Wilson, E. F.; Miras, H. N.; Rosnes, M. H.; Cronin, L. *Angew. Chem., Int. Ed. Engl.* **2011**, *50*, 3720−3724. (c) Miras, H. N.; Stone, D. J.; McInnes, E. J. L.; Raptis, R. G.; Baran, P.; Chilas, G. I.; Sigalas, M. P.; Kabanos, T. A.; Cronin, L. *Chem. Commun.* **2008**, 4703−4705. (d) Miras, H. N.; Long, D.-L.; Kögerler, P. F.; Cronin, L. *Chem. Commun.* **2009**, 1297−1311.
(37) Steiner, T. *Angew. Chem., Int. Ed. Engl.* **2002**, *41*, 48.
(38) Rappé, A. K.; Berstein, E. R. *J. Phys. Chem. A* **2000**, *104*, 6117−6128.